Defense Technical Information Center Compilation Part Notice

ADP023824

TITLE: Accelerated Modeling and New Ferroelectric Materials for Naval SONAR

DISTRIBUTION: Approved for public release, distribution unlimited

This paper is part of the following report:

TITLE: Proceedings of the HPCMP Users Group Conference 2004. DoD High Performance Computing Modernization Program [HPCMP] held in Williamsburg, Virginia on 7-11 June 2004

To order the complete compilation report, use: ADA492363

The component part is provided here to allow users access to individually authored sections of proceedings, annals, symposia, etc. However, the component should be considered within the context of the overall compilation report and not as a stand-alone technical report.

The following component part numbers comprise the compilation report:
ADP023820 thru ADP023869

Accelerated Modeling and New Ferroelectric Materials for Naval SONAR

Ilya Grinberg, Valentino R. Cooper,
Young-Han Shin, and Andrew M. Rappe
*The Makineni Theoretical Laboratories,
Department of Chemistry, University of
Pennsylvania, Philadelphia, PA*
{ilya, vacooper, hyshin,
rappe}@sas.upenn.edu

Thomas J. Baring
*Arctic Region
Supercomputing Center
(ARSC), Fairbanks, AK*
baring@arsc.edu

Sam B. Cable
*USACE Engineer
Research and
Development Center
(ERDC), Vicksburg, MS*
Sam.B.Cable@erdc.usace.
army.mil

Abstract

We have computationally designed new materials for use in Naval SOund NAvigation Ranging (SONAR). Our quantum-mechanical studies show that these lead-free, non-toxic oxides will be high-performance piezoelectrics with promise for use in Naval SONAR and communications applications. To enable this research, we also present techniques for greatly accelerated modeling of oxide materials. We show that a simple atomistic model accurately reproduces our quantum-mechanical results yet is thousands of times faster. We also report successful porting and performance tuning of our computer codes to the CRAY X1, resulting in a great speed-up over previous architectures.

1. Introduction

Perovskite oxides (with formula ABO_3) have a wide range of structural, electrical, and mechanical properties, making them vital materials for many technological applications, such as ultrasound machines, cell phones, and computer memory devices. Perovskite solid solutions with a high piezoelectric response are of particular interest as they can be employed as sensors in SONAR devices. When such a material is deformed by underwater sound vibrations, it generates an electric field which can then be interpreted by a computer to gain information, such as depth and distance. This information is crucial for the defense and operation of Naval submarines and vessels. Other examples of perovskite oxide applications that are vital in the challenging operating conditions of the military include non-volatile ferroelectric memory for safe storage of information, and dielectric materials with tunable resonant frequency and high signal-to-noise ratio for communications devices.

Most of these materials are complex systems with some degree of disorder, making them challenging to study experimentally and theoretically. However, as it is their complexity which gives them their favorable properties, highly accurate modeling which captures the essential features of the disordered structure is necessary to explain the behavior of current materials and predict favorable compositions for new materials. Recently, a combination of methodological improvements and a rise in computer speed has made first-principles calculations a viable tool for understanding these complex systems. In particular, the density functional theory (DFT) approach[1,2] offers a combination of accuracy and computational speed that can reveal the microscopic structure and interactions of complex systems[3-5].

Rational design of new materials with improved properties requires simulations that are accurate and efficient at the length scale of the processes that underlie the desired properties and that are performed at typical device operation temperatures. This creates a "length scale gap" and a "temperature gap" between the desired processes and the DFT modeling of ferroelectric oxides that is typically done for relatively small unit cells and at low temperatures. We bridge these gaps with two strategies. First, we develop correlations between low temperature local properties computed with DFT calculations and macroscopic observables such as the ferroelectric to paraelectric transition temperature. We also develop an atomistic model based on first-principles calculations that allows us to do accurate simulations at finite temperatures and at the nanoscale. Using the discovered correlations between microscopic and macroscopic oxide properties, we computationally design new environmentally friendly high performance piezoelectric and dielectric materials. We also report our success in porting and performance tuning our codes for the Cray X1 platform.

2. Methodology

For all the DFT calculations presented here we use a plane-wave basis set. Such a basis set is complete and offers the advantage of carrying out operations in both real space and reciprocal space through the use of fast Fourier transforms. Calculations are done using the standard LDA[6] exchange-correlation functional using our in-house plane wave code. To reduce the computational cost of the calculations we use designed non-local[7], optimized[8] pseudopotentials to represent the interactions of the nucleus and the core electrons with the valence electrons. Minimization of the energy with respect to the electronic degrees of freedom is done using the blocked-Davidson[9] iterative diagonalization procedure[10] with Pulay density mixing[11]. Ionic minimization is performed using a quasi-Newton algorithm[12]. DFT calculations are performed on supercells of up 60 atoms, with a variety of atomic configurations examined to ensure accurate modeling of the disordered perovskite structures. Molecular dynamics calculations were performed using the MOLDY package[13].
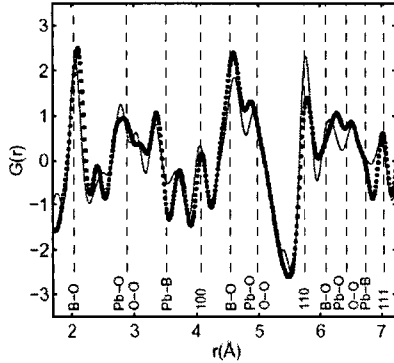

Figure 1. Pair distribution function of DFT simulated structure of PbSc$_{2/3}$W$_{1/3}$O$_3$ (solid line) in comparison with the experimental data (dots)[18]. The close agreement demonstrates that our calculations capture the behavior of this complex material. Similar agreement is obtained for other compositions as well.

3. Results

3.1. Structure Property Correlations in Pb based solid Solutions.

First-principles calculations have proved to be widely useful in obtaining a microscopic understanding of the mechanisms underlying cation ordering[14], phase transitions[3,15] and piezoelectricity[4,16,17] in complex ferroelectric solid solutions. However, reliable prediction of ferroelectric to paraelectric transition temperature T_c from first principles remains to be achieved and the

microscopic mechanisms underlying high T_c (or the related temperature maximum of the dielectric constant) are currently unclear. Here we present our study of the correlations between local structures at the atomic level as determined by DFT calculations and experimentally observed transition temperatures[18–20]. We perform our simulations on PbZr$_{1-x}$Ti$_x$O$_3$ (PZT), $(1-x)$PbMg$_{1/3}$Nb$_{2/3}$O$_3$–xPbTiO$_3$ (PMN-PT) and $(1-x)$PbZn$_{1/3}$Nb$_{2/3}$O$_3$–xPbTiO$_3$ (PZN-PT) solid solutions that form the core of current and next-generation Navy SONAR devices. We also study the related systems $(1-x)$PbSc$_{2/3}$W$_{1/3}$O$_3$–xPbTiO$_3$ (PSW-PT), $(1-x)$PbSc$_{2/3}$W$_{1/3}$O$_3$–xPbZrO$_3$ (PSW-PZ), and PbSc$_{1/2}$Nb$_{1/2}$O$_3$ (PSN). Our modeling of local structure is accurate, as indicated by excellent agreement between pair-distribution functions obtained from DFT calculations and by neutron scattering[18] (Figure 1).

We find that there is a strong relationship between the low-temperature polarization P (as found by our DFT calculations) and the experimentally obtained temperature T_c at which the dielectric constant is maximum:

$$T_c = \gamma P^2, \tag{1}$$

where γ is a constant. Figure 2 shows the correlation between the transition temperatures predicted by Eq. 1 and those from experimental data. The slope of the least square fitted curve guiding the eye is 1.1, indicating that Eq. 1 accurately and quantitatively captures the trends in transition temperatures among these fairly different systems.

The correlation presented in Figure 2 can be explained based on the simple Landau theory for ferroelectric crystal. The free energy is

$$G = G_0 + \alpha(T - T_c)P^2 + \beta P^4 \tag{2}$$

where G_0 is the free energy of the high-symmetry paraelectric phase, α and β are constants and P is polarization. The equilibrium polarization at a given temperature T is

$$P^2 = \alpha(T_c - T)/2\beta. \tag{3}$$

Substituting $T = 0$ used in our DFT calculations and solving for T_c, we obtain

$$T_c = 2\beta P^2/\alpha, \tag{4}$$

relating the T_c to the square of computed polarization. The high quality of the fit in Figure 2 means that for the Pb-based perovskites examined here the ratio β/α is nearly constant and can be approximated by β/α=635 Km^4/C^2.
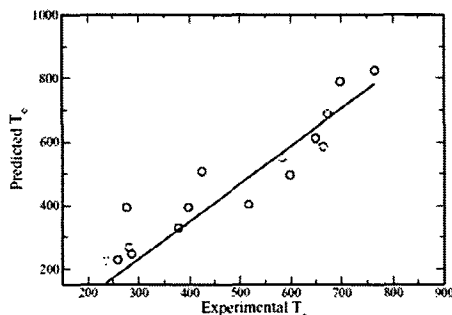
Figure 2. Correlation between transition temperatures predicted by Eq. 1 (γ =1270 Km^4/C^2) and obtained experimentally for a variety of Pb-based solid solutions. The close match means that we can now predict transition temperature from low-temperature calculations.

The linkage between the microscopic properties computed with accurate first-principles calculations and T_c makes possible the rational design of high T_c piezoelectrics. Fundamentally, we have shown that the behavior of individual ions in heterovalent perovskite ferroelectric solid solutions can be directly linked to local structure and macroscopic collective properties

3.2. Bond Valence Model – Efficiently Modeling Complex Oxides.

While some properties of ferroelectric materials are due to the local, Angstrom-scale structure, others are dependent on behavior at longer length and time scales. Domain wall motion, crucial for non-volatile ferroelectric memory applications, is an excellent example of a technologically important but poorly understood nanoscale process. Highly accurate simulations are needed to obtain a quantitative microscopic understanding of such processes. The prohibitive cost of a first-principles calculation on such a large system necessitates development of computationally inexpensive, yet accurate interatomic potentials for molecular dynamics simulations.

In this paper, we present an atomistic model for the molecular dynamics study parameterized from first-principles calculations and show the ferroelectric phase transition of bulk $PbTiO_3$ crystal and the domain wall energy of 180° $PbTiO_3$ domains. Our potential model follows the bond-valence theory[21] developed from experimental crystallographic data for many oxide systems. The valence of an atom is assumed to be distributed among the bonds it forms, and the resulting valence (the "bond valence") correlates with the bond length through an inverse power relation. In other words, the sum of bond valences at each atom is equal to the atomic valence. The validity of the bond-valence (BV)

theory for ferroelectric oxides was proved in our previous work[3, 22].

The reference structures were obtained from the *ab initio* density functional theory molecular-dynamics calculations on a small supercell. About 2000 reference structures were obtained, and 25 of those were selected for the fitting database. To obtain the bond-valence model potential parameters, we used the simulated annealing global optimization method to minimize the difference between the BV and DFT energies and atomic forces for the structures in the database. The BV model with optimized parameters was then tested against all 2000 reference structures, showing good agreement with DFT results as shown in Figure 3.
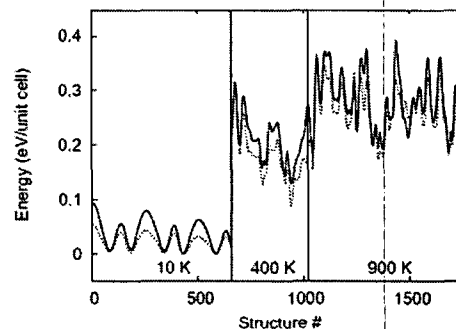

Figure 3. Energies of various oxide structures computed by DFT (dotted) and by bond-valence model calculation with optimized parameters (solid line)

We then performed molecular dynamics simulations with the BV model at a variety of temperatures in the NVT ensemble using the experimental lattice constants[23]. In agreement with this experiment we find that as temperature increases, polarization P decreases. Using a relatively small 3×3×3 MD cell, we find a ferroelectric to paralectric phase transition at around 600K. The phase transition is of mixed order-disorder and displacive type, in agreement with experimental data[24]. As the size of the simulation cell is increased to 5×5×5 and 7×7×7, the ferroelectric-to-paraelectric phase transition temperature increases to 650K and 680K respectively. The transition temperature for the largest simulation cell agrees well with the experimental value of 765K. Comparison of temperature dependence of polarization with experimental data also shows good agreement[25] (Figure 4).
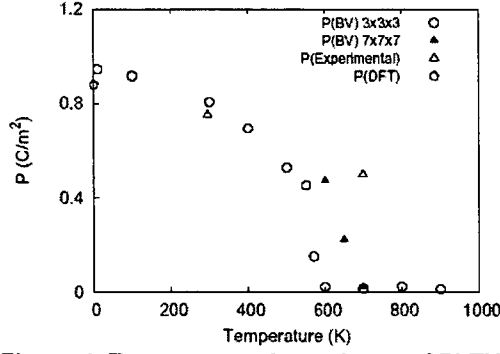
Figure 4. Temperature dependence of PbTiO₃ polarization. Our model predicts a ferroelectric to paraelectric phase transition at T_c =680K, in good agreement with experimental c =765K. Experimental lattice constants for a and c axes were used at each temperature. Open circles are the polarization for the 3×3×3 MD cell and solid triangles are the polarization for the 7×7×7 MD cell.

To test the accuracy of our potential for the study of domain wall motion in non-volatile memory devices, we computed the energy of the 180° domain wall. We find that domain wall energy in excellent agreement with DFT data (Table 1). Since our BV parameterization database did not contain any domain wall structures, the excellent agreement between BV and DFT methods is another strong indicator that our BV model correctly captures the essential physics of PbTiO₃.

Table 1. Comparison of experimental, DFT and BV data for PbTiO₃. Polarization P in C/m², domain wall energy in mJ/m² and transition temperature T_c in Kelvin.

	P 10K	P 300K	Domain Wall Energy	T_c
BV	0.92	0.80	140	680
DFT	0.88	–	152	–
Exp.	–	0.75	–	765

Our development of a highly efficient yet very accurate atomistic model for PbTiO₃ creates an opportunity for study of a variety of technologically important nanoscale processes. We are now working on techniques to enable simulations at the mesoscale.

3.3. DFT Study of Non-toxic Piezoelectrics.

Our previous work showed that Ag ions display off-centering behavior crucial to high piezoelectricity when alloying with PbTiO₃ eliminates B-O₆ octahedral rotations[26]. Building on our previous computational materials design studies, we further investigated the properties of xAgNbO₃-(1 – x)PbTiO₃ (ANPT) ferroelectric solid solutions as well as the properties of the

lead free, environmentally friendly xAgNbO₃-(1−x)BaTiO₃ (ANBT) solid solutions.

We look for compositions which exhibit improvement over the current PZT or BaTiO₃ (BT) piezoelectrics in three desired properties: piezoelectric performance, T_c and lower toxicity. In order to determine if the proposed materials are likely to be good piezoelectrics, we examine P values and the energy difference between rhombohedral (R) and tetragonal (T) phases (ΔE_{R-T}). Materials with large P will couple strongly to an applied electric field; a small ΔE_{R-T} indicates the presence of a monoclinic (M) phase at the morphotropic phase boundary (MPB) crucial for easy polarization rotation and high piezoelectric performance[4,27]. High T_c is favored by a large energy difference between the distorted polarized structure and the non-polar high symmetry structure (ferroelectric instability ΔE_{FE}) and high polarization, and high T_c is disfavored by large octahedral rotations[28,29]. Elimination of Pb atoms from the A-site makes a material environmentally-friendly. The results for ΔE_{R-T} are presented in Figure 5, and P magnitudes, ΔE_{FE} values and average O₆ rotation angles at MPB of each solution are presented in Table 2.
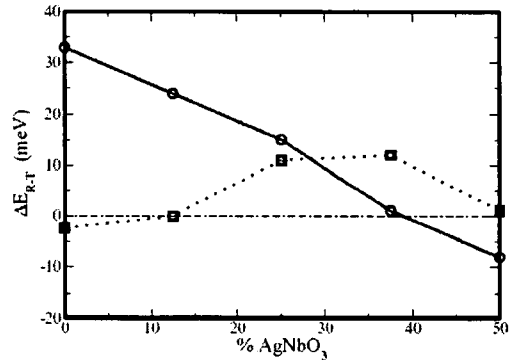

Figure 5. Energy difference between rhombohedral and tetragonal phases as a function of AgNbO₃ content for ANPT (solid) and ANBT (dotted) solid solutions. Positive ΔE_{R-T} values indicate that tetragonal phase is preferred. Morphotropic phase boundaries are present when ΔE_{R-T} crosses 0 at 37.5% AN content for ANPT system and at 12.5% and 50% for ANBT system.

Table 2. Results of DFT calculations for compositions of ANPT and ANBT solid solutions closest to MPB. Results for BT and 50/50 PZT are given for comparison. The new ANBT materials are lead-free with piezoelectricity on par with PZT. MPB content is in percent, P and ϵ_{33} magnitudes are in C/m^2, ΔE_{FE} values are in meV per 5-atom cell, average O$_6$ rotation angles are in degrees. The values for 50/50 PZT are taken from References 17, 20, and 26.

	% AN at MPB	P	ΔE_{FE}	O$_6$ rot angle	Lead Free	ϵ_{33}
BT	–	0.24	16	0.0	Y	5.3
PZT	–	0.64	117	2.0	N	12.6
ANPT	37.5	0.60	45	7.7	N	9.2
ANBT	12.5	0.32	48	0.4	Y	9.5
ANBT	50.0	0.44	26	5.0	Y	14.5

We find that while the ANPT system should exhibit good piezoelectric performance, the T_c most likely will not be higher than that of current PZT materials. Our calculations predict a standard phase diagram[30] with a T → M → R sequence of phase transitions with decreasing PT content and a M phase around 37.5% AN composition. The large 0.6 C/m^2 P at MPB is promising for good piezoelectric performance. However, T_c at MPB will most likely be significantly the PT T_c due to a decrease in ΔE_{FE} and large O$_6$ rotations (7.7° versus 2.0° in 50/50 PZT[22]). Finally, the presence of the Pb atoms on the A-site makes this proposed material environmentally unfriendly and difficult to synthesize in a pure bulk form due to formation of the competing pyrochlore phase commonly found in perovskites that contain both Pb and Nb[31].

Our results for the ANBT system indicate that it is a promising candidate for high performance lead-free piezoelectrics. This system has a rich phase diagram with an unusual R → M → T → M → R phase transition sequence, which is due to volume expansion effects. In a solid solution, alloying a perovskite of a small volume into a perovskite of large volume expands the A site for the smaller A-cation. This can be thought of as applying negative pressure to the smaller perovskite. Tetragonality of the solid solution is favored both by a larger negative pressure[32,33], (i.e., a larger average system volume), and by a greater fraction of the smaller A-cation sites under negative pressure. Since these two effects have opposite dependence on AN concentration, ΔE_{R-T} can be expected to exhibit non-monotonic dependence on AN content, as is observed in our DFT calculations. The two MPBs are located at 12.5% and 50% AN content, with P values enhanced relative to BT and comparable to the P of some of the current single crystal lead based materials[34].

For both MPB compositions, ΔE_{FE} values are significantly increased relative to BT, with small O$_6$ rotations for the 12.5% AN composition; for 50% AN

composition the 5° rotations are larger than 2° rotations found in 50/50 PZT[22]. For these two promising compositions, we also computed the e_{33} piezoelectric coefficients. The computed e_{33} values were 9.5 C/m^2 and 14.5 C/m^2 for the 12.5% AN and 50% AN compositions respectively. These values are comparable to the 12.6 C/m^2 computed and 11.6 C/m^2 measured for 50/50 PZT solid solution[17]. In summary, we have shown that Ag cations can be ferroelectrically active on the perovskite A-site. Alloying AgNbO$_3$ with PbTiO$_3$ leads to a standard phase diagram with an MPB around 37.5% AgNbO$_3$ composition. An unusual phase diagram is obtained for the AgNbO$_3$-BaTiO$_3$ solution, with excellent piezoelectric properties at the two MPB locations. The ANBT solid solutions should also display a higher T_c than BaTiO$_3$. The low toxicity and excellent piezoelectric properties make ANBT solid solutions promising materials for experimental investigation.

3.4. DFT Based Design of New Dielectric Materials.

Besides applications utilizing their ferroelectric properties, perovskite materials are also widely use as dielectrics in telecommunications applications. There is a current need for materials that have a high tunability (ability to change their dielectric constant and resonant frequency with an applied electric field), but also low dielectric loss (increased signal-to noise ratio). The current state of the art tunable, low-loss dielectrics are based on incipient ferroelectrics. These materials have a very shallow ferroelectric instability, typically develop polarization only at very low temperature and are paraelectric at room temperature. The flat potential energy surface gives these materials the ability to develop a large polarization with an applied electric field, leading to a large dielectric constant. Current dielectrics such as KTa$_{1-x}$Nb$_x$O$_3$, AgTa$_{1-x}$Nb$_x$O$_3$ and Ba$_{1-x}$Sr$_x$TiO$_3$ are all B-site based, with the B-cations providing the off-centering and polarization under applied electric fields. Here, we examine the possibility of alloying end-member materials that are not incipient ferroelectrics to give rise to an A-site based incipient ferroelectric solid solution, using the xAgNbO$_3$-(1−x)BaZrO$_3$ (ANBZ) system as a test case.

BaZrO$_3$ is a low-loss dielectric with a volume that is 22% larger than that of AgNbO$_3$. Recent theoretical calculations have shown that large perovskite volume expansion under "negative pressure" leads to an anomalous increase in tetragonality and very large cation displacements[32,33]. Alloying AN with BZ is a way of realizing such negative pressure experimentally. Our calculations on the AN-BT system also suggest that volume expansion effects are favorable for ferroelectricity in the Ag-based systems.

Data in Table 3 show that alloying just 12.5%AN into BZ leads to a development of small polarization, typical of incipient ferroelectrics at very low temperatures[35]. The polarization is due to a combination of large Ag off-centering and small displacements by the other cations. The large Ag displacements are due to a volume expansion of the AgO_{12} cage which creates a deep instability in the Ag potential energy surface. The small, but non-zero distortions of the Ba, Zr and Nb cations indicate that the volume-expansion induced Ag displacements soften the local potential felt by the Ba, Zr and Nb cations, creating a very shallow double well similar to the shallow double well found in $SrTiO_3$ incipient ferroelectric.

Table 3. Results of DFT calculations for ANBZ solid solution. Displacements in Å, P magnitudes are in C/m^2, ΔE_{FE} values are in meV per 5-atom cell, average O_6 rotation angles are in degrees.

	Ag disp	Ba disp	Zr/Nb disp	O_6 rot angle	P	ΔE_{FE}
0.0 AN		0.00	0.00	0.0	0.0	0
12.5 AN	0.89	0.06	0.05	3.3	0.11	59
25 AN	0.84	0.06	0.07	3.4	0.19	64
37.5 AN	0.64	0.06	0.08	5.9	0.24	34
50 AN	0.44	0.07	0.06	8.1	0.20	24

Examination of the data for the other AN compositions shows that the AN-BZ solid solution displays an interesting C → T → M → O sequence of 0 K compositional phase transitions and a nonmonotonic dependence of ΔE_{FE} on AN content, due to volume effects as explained above for the AN-BT solid solution. The octahedral tilt angle shows an increase from 0° at pure BZ to 8.1° at 50/50 ANBZ composition. Large tilt angles in perovskites have been correlated with large dielectric loss[36], indicating that dielectric loss will increase with AN content as well. Taken together, the correlations between incipient ferroelectricity and high tunability, and between low dielectric loss and low octahedral tilt angle suggest that 12.5% and 25% AN-BZ compositions are good candidate low-loss, frequency-agile materials.

3.5. Cray X1 Port.

During the course of the past year, we have ported our plane-wave code to the X1 platform. Our program contains approximately 9,500 lines of code and makes calls to several mathematical libraries, making the porting and optimizing performance a non-trivial task. The results for several benchmarks were tested and compared against typical production platforms such as Pentium 4 Xeon Beowulf Cluster and the SGI O3K computers. Agreement to six decimal places between the X1 and

other platforms was achieved. As expected, proper vectorization and optimal memory usage were crucial for taking advantage of the Cray X1 architecture. After the code was fully vectorized, a speed-up of 9.2 times over Pentium 4 Xeon and 6.6 times over the SGI O3K was achieved. We are currently using the X1 in production mode and working on optimizing scratch disk and memory usage to get further speed-up.

4. Significance to DoD

The perovskite oxides are used extensively in modern Naval SONAR devices, non-volatile memories and telecommunications applications. The US Navy would reap a considerable military advantage from developing SONAR-detecting materials and microwave materials with higher performance, lower cost and less harmful environmental side effects. Understanding the behavior of current perovskite oxides is critical for the goal of developing new materials. Once the relationship between the atomic composition, structure and materials properties are understood, new materials that improve upon existing technology can be designed. Our DFT calculations have revealed the microscopic origin of transition temperature which sets the operating range of piezoelectric devices, and our development of the bond-valence modeling approach will be of great benefit to the study of processes on nano-and mesoscales in non-volatile ferroelectric memory and relaxor piezoelectrics used in the devices of the next decade. Our ANBT and ANBZ work identifies promising candidates for environmentally-friendly high performance piezoelectrics and dielectrics.

5. Systems Used

ERDC SGI3900 and Cray X1, ARSC Cray SX-6 and X1, and AHPCRC Cray X1.

6. CTA

Computational Materials Science (CMS)

References

1. Hohenberg, P. and W. Kohn, *Phys. Rev.*, 136, B864, 1964.

2. Kohn, W. and L.J. Sham, *Phys. Rev.*, 140, 1965, A1133.

3. Grinberg, I., R. Cooper, and A.M. Rappe, *Nature*, 419, 2002, 909.

4. Fu, H. and R.E. Cohen, *Nature*, 402, 2000, 281.

5. George, A.M., J. Iniguez, and L. Bellaiche, *Nature*, 413, 2001, 54.

6. Perdew, J.P. and A. Zunger, *Phys. Rev. B*, 23, 1981, 5048.

7. Ramer, N.J. and A.M. Rappe, *Phys. Rev. B*, 59, 1999, 12471.

8. Rappe, A.M., K.M. Rabe, E. Kaxiras, and J.D. Joannopoulos, *Phys. Rev. B Rapid Comm.*, 41, 1990, 1227.

9. Davidson, E.R., *J. Comput. Phys.*, 17, 1975, 87.

10. Bendtsen, C., O.H. Nielsen, and LB. Hansen, *Appl. Num. Math.*, 37, 2001, 189.

11. Pulay, P., *J. Comp. Chem.*, 3, 1982, 556.

12. Pfrommer, B.G., M. Cote, S.G. Louie, and M.L. Cohen, *J. Comp. Phys.*, 131, 1997, 233.

13. MOLDY is developed by Keith Refson, and it is free software following the terms of the GNU General Public License.

14. Cockayne, E. and B.P. Burton, *Phys. Rev. B*, 60, 199, R125429.

15. Bellaiche, A.G.L. and D. Vanderbilt, *Phys. Rev. B*, 84, 200, 54270.

16. Saghi-Szabo, G. and R.E. Cohen, *Phys. Rev. B*, 59, 1999, 12771.

17. Wu, Z. and H. Krakauer, *Phys. Rev. B*, 68, 2003, 14112.

18. Juhas, P., W. Dmowski, I. Grinberg, T. Egami, A.M. Rappe, and P.K. Davies, *Phys. Rev. B*, in press 2004.

19. Mitsui, T. in *"Oxides"* Landolt-Bornstein, New Series, Group III, Vol. 16, Pt. A, Springer, Berlin, 1981.

20. Bokov, A.A., Y.-H. Bing, W. Chen, Z.-G. Ye, S.A. Bogatina, I.P. Raevski, S.I. Raevskaya, and E.V. Sakhar, *Phys. Rev. B*, 68, 2003, 052102 1.

21. Brown, I.D., *"Structure and Bonding in Crystals II"*, Academic, NY, 1981, pp. 1–30.

22. Grinberg, I., V.R. Cooper, and A. M. Rappe, *Phys. Rev. B*, 69, 2004, 144118.

23. Shirane, G., S. Hoshino, and K. Suzuki, *Phys. Rev.*, 80, 1950, 1105.

24. Egami, T., E. Mamontov, and W. Dmowski, in *"Fundamental Physics of Ferroelectrics 2003"*, edited by P.K. Davies and D.J. Singh, American Institute of Physics, Melville, NY, 2003, pp. 48–53.

25. Gavrilyachenko, V.G., *Sov. Phys. Solid State*, 12, 1970, 1203.

26. Grinberg, I. and A.M. Rappe, in *"Fundamental Physics of Ferroelectrics 2003"*, edited by P.K. Davies and D. J. Singh, American Institute of Physics, Melville, NY, 2003, pp. 130–138.

27. Guo, R., L.E. Cross, S.-E. Park, B. Noheda, D.E. Cox, and G. Shirane, *Phys. Rev. Lett.*, 84, 2000, 5423.

28. Fornari, M. and D.J. Singh, *Phys. Rev. B*, 63, 2001, 092101 1.

29. Iniguez, J. and D. Vanderbilt, *Phys. Rev. B*, 67, 2003, 224107.

30. Cox, D.E., B. Noheda, G. Shirane, Y. Uesu, K. Fujishiro, and Y. Yamada, *Appl. Phys. Lett.*, 79, 2001, 400.

31. Davies, P.K., private communication, 2003.

32. Tinte, S., K.M. Rabe, and D. Vanderbilt, *Phys. Rev. B*, 68, 2003, 144105.

33. Halilov, S.V., M. Fornari, and D.J. Singh, *Appl. Phys. Lett.*, 81, 2002, 3443.

34. Zhang, S.J., S. Rhee, C.A. Randall, and T.R. Shrout, *Jpn. J. Appl. Phys.*, 41, 2002, 722.

35. Itoh, M., R. Wang, Y. Inaguma, T. Yamaguchi, Y.-J. Shan, and T. Nakamura, *Phys. Rev. Lett.*, 82, 1999, 3540.

36. Levin, I., T.G. Amos, S.M. Bell, L. Farber, T.A. Vanderah, R.S. Roth, and B.H. Toby, *J. Solid State Chem.*, 175, 2003, 170.